Lifetime measurement of excited states in ^{144}Ce: Enhanced $E1$ strengths in a candidate for octupole deformation

M. Beckers,[*] C. Müller-Gatermann, A. Blazhev, T. Braunroth, A. Dewald, C. Fransen, A. Goldkuhle,
L. Kornwebel, J. Litzinger, F. von Spee, and K.-O. Zell

Institut für Kernphysik der Universität zu Köln, Zülpicher Str. 77, D-50937 Köln, Germany

A lifetime measurement of excited states in ^{144}Ce using the ^{142}Ce(^{18}O, ^{16}O) reaction with a beam energy of 67 MeV and the recoil distance Doppler-shift method was performed at the Cologne FN Tandem accelerator. Lifetimes of the three lowest yrast states in ^{144}Ce have been measured as well as for the 3_1^- state and an effective lifetime of the 4_2^+ state. Reduced $E2$ transition strengths determined using these results have been compared to predictions from recent shell-model calculations. From the interband transitions reduced $E1$ strengths could be determined, which are strongly enhanced.

I. INTRODUCTION

The $^{144}_{58}$Ce$_{86}$ nucleus is located on the neutron-rich side of the valley of stability, close to $N = 88$, a nucleon number that is related to interesting phenomena throughout the nuclear chart. On the one hand a shape phase transition is expected at $N = 88$–90 for nuclei in the Ba-Dy region [1]. Such transitions have been of major interest in nuclear physics research for a long time. Especially, a phase transition from spherical to deformed is expected between ^{146}Ce and ^{148}Ce, which was the object of extensive studies in recent work [2]. Knowledge about ^{144}Ce in the close vicinity would provide helpful information regarding the onset of deformation in that region. On the other hand also the phenomenon of octupole deformation plays an important role in the $N \approx 88$, $Z \approx 56$ region. At these nucleon numbers nuclei are especially prone to octupole correlations [3]. This is explained with a strong octupole coupling between the $h_{11/2} \leftrightarrow d_{5/2}$ and the $i_{13/2} \leftrightarrow f_{7/2}$ single-particle orbitals, respectively [4]. Experimentally, octupole deformation was related to alternating parity bands and low-lying negative-parity band heads. Such bands are reported in several lanthanide nuclei, including ^{144}Ce [5]. Experimental indications for such a deformation apart from the band structure are enhanced $E1$ and $E3$ transition strengths. Direct evidence for octupole deformation was obtained for ^{144}Ba by measuring $E3$ transition strengths [6]. For comparison the partial level scheme of ^{144}Ce is shown together with the ones of ^{144}Ba and ^{142}Ba in Fig. 1. These clearly show the typical structure of the supposed octupole bands, which is exhibited in each of these nuclei.

Aside from the $2_1^+ \rightarrow 0_{gs}^+$ transition, no transition strengths are experimentally known for ^{144}Ce. To shed some light on the question of octupole deformation it would be most helpful to measure $E3$ transition strengths in ^{144}Ce. However, because

up to now no $E3$ transitions have been observed, the experiment that is presented here aims to get information about the $B(E1)$ values via transitions connecting positive and negative parity states. While enhanced $E1$ transition strengths can also be indicators for octupole deformation, lifetime information of negative parity states are essential to deduce $E3$ transition strengths, for example, if a characteristic $3_1^- \rightarrow 0_{gs}^+$ transition will be observed in future experiments. Level lifetimes are also very important as model independent input parameters in the analysis of Coulomb excitation experiments, which can deduce $E3$ matrix elements also for nonobserved transitions. In addition, the $B(E2)$ values between yrast states provide important insights into the general collective structure of the nucleus, especially by comparing them to theoretical model predictions.

II. EXPERIMENT

The presented experiment was performed at the Institute for Nuclear Physics at the University of Cologne. Excited states in ^{144}Ce were populated by the 2n transfer reaction ^{142}Ce(^{18}O, ^{16}O). The beam was delivered by the Cologne FN Tandem Accelerator with a beam energy of 67 MeV. To measure the lifetimes of excited states, the target foil, consisting of 0.5 $\frac{mg}{cm^2}$ ^{142}Ce on a 1.2 $\frac{mg}{cm^2}$ Ta support layer facing the beam, was mounted in the Cologne Plunger device [9]. At the stopper position a 4.1 $\frac{mg}{cm^2}$ Nb foil was installed, which was sufficient to stop the recoiling nuclei with an average velocity of $v/c = 1.57(1)\%$. The plunger device is used to set different target-to-stopper distances and to keep them constant by measuring the target-stopper capacitance and compensate for drifts using a piezoelectric device. Emitted γ rays were measured by 11 large volume Germanium detectors with relative efficiencies between 55% and 83%, arranged in two rings, ring 1 (six detectors at 45°) and ring 2 (five detectors at 142.3°). Additionally an array of six solar cells, covering the solid angle between 117° and 167°, was used to measure
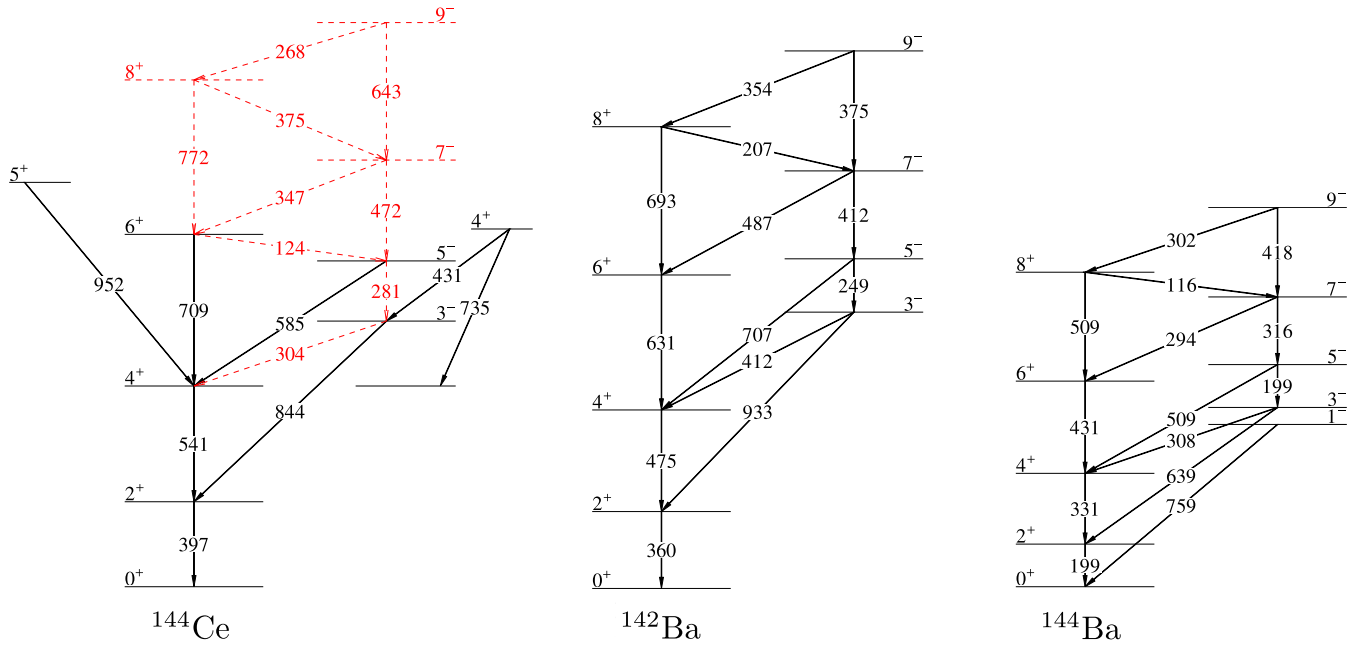
___

*mbeckers@ikp.uni-koeln.de

FIG. 1. Partial level schemes of ^{144}Ce, ^{142}Ba, and ^{144}Ba. Transition energies are given in keV. For ^{144}Ce the transitions observed in this experiment are shown in black while levels and transitions shown with dashed red lines have been observed in earlier experiments [5,7] and are included to display the mentioned interspacing of positive and negative parity states with the respective interband transitions. Data for ^{142,144}Ba were taken from [8]. See text for details.

backscattered particles to select the reaction channel using a particle-γ coincidence gate. All detector angles are given with respect to the beam axis. During the course of the experiment data for a total of eight different target-to-stopper distances between 21 μm and 364 μm were taken. The absolute reaction cross section for the used 2n-transfer reaction could not be obtained, because the decays of ^{144}Ce are not observable without using a gate on the backscattered particle. Therefore only an effective reaction cross section can be given, i.e., the cross section for the case when the ^{16}O reaction partner is scattered into the solid angle between 117° and 167° and detected by the solar cells. With an estimated average beam current of about 6.5×10^9 pps for a single run the effective cross section for the $2_1^+ \rightarrow 0_{gs}^+$ transition in ^{144}Ce was calculated to be about 3 mb. The effective cross section of the 2n transfer in relation to Coulomb excitation, also for the respective $2_1^+ \rightarrow 0_{gs}^+$ transitions is given by the intensity ratio,

$$\frac{I_{2^+}(2n)/\epsilon(E)}{I_{2^+}(\text{CoulEx})/\epsilon(E)} \approx 0.12,$$

where $\epsilon(E)$ is the detector efficiency for the respective transition energy. It has to be noted that no angular correlations were taken into account.

III. LIFETIME ANALYSIS

Spectra for the data analysis were created by employing particle-γ coincidence gates to select the nuclear reaction of interest. However, from the spectrum of backscattered particles it was not possible to distinguish between ^{16}O and ^{18}O. Therefore also excited states in ^{142}Ce, populated through Coulomb excitation, are visible in the respective particle-

gated spectra (see Fig. 2). Using γ-γ coincidences for this analysis was not possible, because the number of coincident events is far too low, owing to the low cross section of the production reaction.

For the three lowest positive parity yrast states the development of the unshifted and shifted component of the decay is clearly visible for the various plunger distances. Spectra of three different distances (small, medium, long) are shown for these three states in Fig. 3. To determine lifetimes of the 2_1^+ and the 4_1^+ excited states in ^{144}Ce, the well-established differential decay curve method (DDCM) for the analysis of recoil distance Doppler-shift (RDDS) measurements in its γ-single implementation was used. A detailed review of this method is given in Ref. [9].

Following the DDCM the lifetime of a given state is obtained via

$$\tau_i(x) = \frac{-R_i(x) + \sum_k b_{ki}\alpha_{ki}R_k(x)}{\frac{d}{dx}R_i(x)} \times \frac{1}{v}, \quad (1)$$

where R_i and R_k denote the decay curves of the state of interest (i) and the feeding states (k), respectively. These can be obtained from the depopulating γ transitions. The velocity of the recoil is denoted as v and x is the target-to-degrader separation, while α_{ki} is a proportionality factor determined by the detector efficiency and the angular distribution of the γ rays and b_{ki} is the branching ratio. Thus the intensities of the depopulating transitions as well as the ones of all observed populating transitions are needed for the lifetime analysis and a careful investigation of the feeding had to be carried out. In total, two feeding transitions were observed for the 2_1^+ state ($4_1^+ \rightarrow 2_1^+$, $3_1^- \rightarrow 2_1^+$) while four such transitions were found for the 4_1^+ state ($6_1^+ \rightarrow 4_1^+$, $5_1^- \rightarrow 4_1^+$, $5_1^- \rightarrow 4_1^+$, $4_2^+ \rightarrow 4_1^+$).
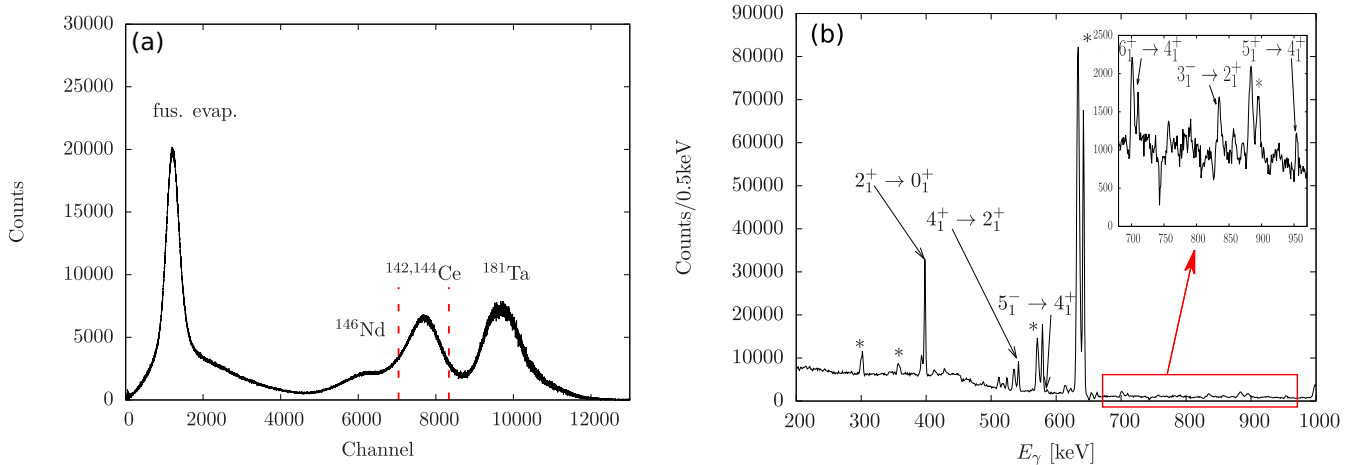
FIG. 2. (a) Particle spectrum measured with solar cells. (b) γ-ray energy spectrum as measured with detectors at backward angles in coincidence to the gate indicated in the particle spectrum (dashed lines). Visible transitions investigated in this paper are marked. Other visible peaks originate from states in the contaminant ^{142}Ce nucleus and are marked with asterisks.

As can be seen in Fig. 2 the feeding transition $5_1^- \rightarrow 4_1^+$ is energetically close to a stronger contaminant transition ($4_1^+ \rightarrow 2_1^+$ in ^{142}Ce). Therefore, it is completely overlapped by the flight component of that transition under forward angle detection and thus the spectra of the detectors at a forward angle cannot be used for analyzing the decay of the 4_1^+ state. For the feeding transition depopulating the 5_1^+ state only the stop component was observed at all distances, which leads to the assumption that the lifetime of this 5_1^+ state is long compared to the longest achieved flight time of about 77 ps. A partial level scheme displaying the level feeding observed and taken into account is shown in Fig. 1.

The peak areas of all aforementioned transitions were determined and, after being corrected for detector efficiencies, used to obtain the lifetimes. The τ curves resulting of the lifetime determination process together with the intensities

of the shifted and unshifted γ-ray components are shown in Fig. 4. Note that this figure only shows the results for the backward angle detection. For analyzing the decay of the 2_1^+ state also the detector ring under forward angle was used and the resulting lifetime is given by the weighted average of both rings as $\tau(2_1^+) = 55.1(5)$ ps. The analysis of the 4_1^+ state yielded $\tau(4_1^+) = 9.4^{+0.9}_{-0.4}$ ps. Here the uncertainties are increased beyond the value given in Fig. 1(b) to account for the low statistics of the transitions feeding the 4_1^+ state.

To determine the lifetime of the 6_1^+ state the Bateman equation of its decay was used instead of the DDCM. The reason was, that here only few distances are within the region of sensitivity, which diminishes the advantages of the DDCM. No feeding transitions for the 6_1^+ state were observed. Because transfer reactions typically lead to the population of only the lowest states in a nucleus, this observation is compatible to the justified assumption that the 6_1^+ state is nearly exclusively directly populated. Hence, the Bateman equation for a decay without feeding was used and fitted to the experimentally determined intensity ratios for both detector rings. To determine the uncertainty, a Monte Carlo simulation with 10^6 iterations was employed, where uncertainties of the absolute distances, the recoil velocity, and the intensity ratios were taken into account. The given uncertainties correspond to the 1σ intervals to both sides of the mean value. This method was used for the analytical analysis of RDDS data before, for example, in Ref. [10], and provides an easy way to incorporate all significant sources of uncertainties. The fit as well as the probability distribution are shown in Fig. 5 exemplary for forward angle detection. The extracted lifetimes for both detector rings in this case show some discrepancies, as for the forward ring the resulting lifetime is $4.9^{+1.0}_{-0.7}$ ps while for ring 2 the analysis yields $7.4^{+1.2}_{-0.9}$ ps. The spectra were extensively checked for contaminations that could explain such deviations but none have been found. Because no such discrepancies occur for every other state's analysis, other systematic errors related to treatment of the two rings can be excluded. Therefore the discrepancy is very likely caused by the relatively
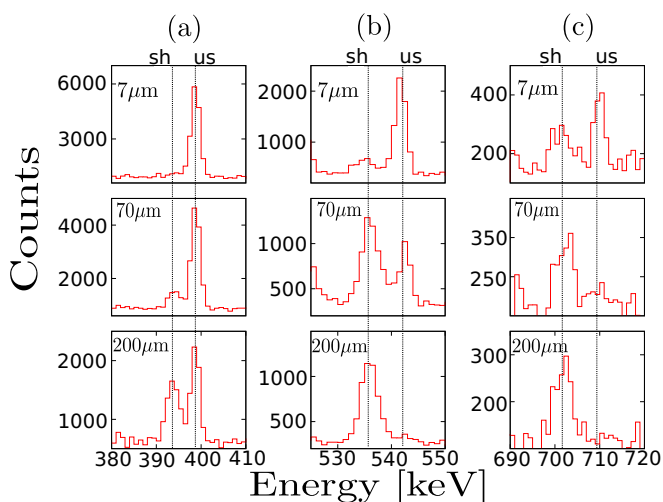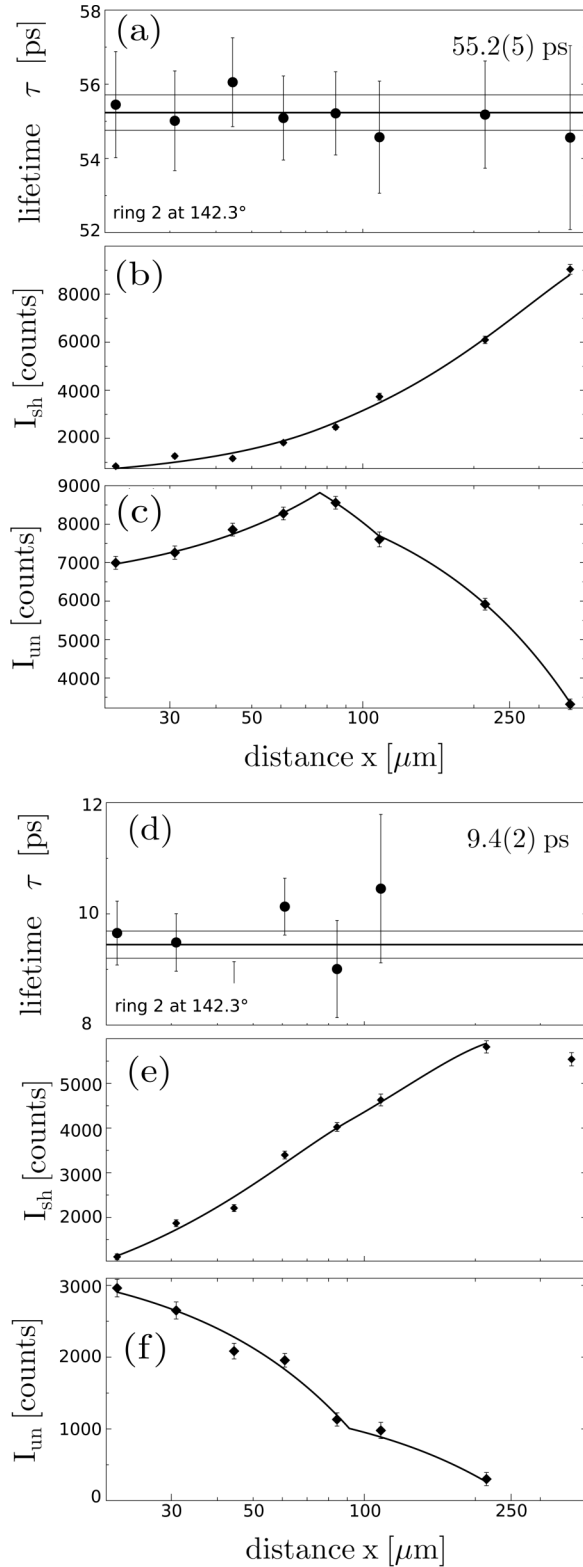

FIG. 3. Spectra of the $2_1^+ \rightarrow 0_1^+$ (a), $4_1^+ \rightarrow 2_1^+$ (b), and $6_1^+ \rightarrow 4_1^+$ (c) decays for three different plunger distances measured under backward angle.

FIG. 4. τ curves of the 2_1^+ state (a) and of the 4_1^+ state (d) together with the respective intensities of the shifted [(b) and (e)] and unshifted [(c) and (f)] components as a function of the target-stopper separation as observed with detectors at backward angles. Uncertainties given here only include statistical uncertainties from the fitting procedure, not from feeding assumptions. Final uncertainties of the lifetimes are given in Table II.
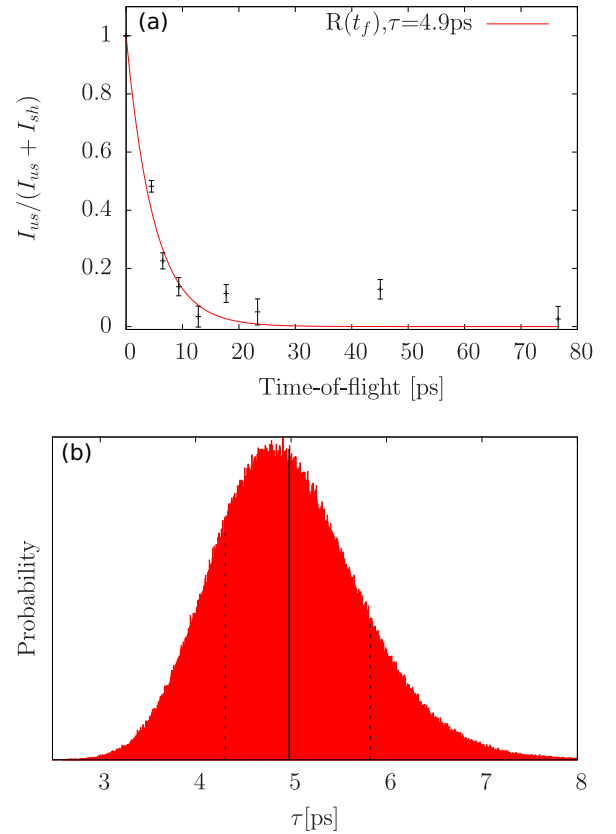

FIG. 5. Decay curve with lifetime fit (a) and probability distribution (b) for the 6_1^+ state; decay observed at forward angles.

low statistics for this decay. To account for this, the variance between the two values was used for the calculation of the uncertainty of the weighted mean. This yields a temporary value of $\tau(6_1^+)_{\text{nofeed}} = 6.2(1.6)\,\text{ps}$. To investigate the assumption that the 6_1^+ state is exclusively populated directly by the reaction, the effects of possible unobserved feeding have been simulated. A realistic amount of unobserved feeding for a "worst-case scenario" can be extrapolated by looking at the feeding of the lower lying states. Because the population of states in transfer reaction is diminished with rising excitation energy, also the amount of feeding in relation to the direct population of a state is reduced for higher excitation energies. Consequently it is justified to assume that the percentage of unobserved feeding for the 6_1^+ state does not exceed the observed feeding of the lower states. It has to be noted that the population of excited states in transfer reactions typically also decreases with level spin. However, the only feeding transitions leading to the population of the 6_1^+ state that have been observed in earlier experiments, for example, in Ref. [11], stem from the 8_1^+ and the 7_1^- states. According to the relative intensities given in Table I an assumption of 20% feeding for the 6_1^+ state should therefore be a sufficiently conservative estimate. For the sake of simplicity the feeding is modeled by a single hypothetical state lying above the 6_1^+. The effective lifetime of that state was chosen to be 100 ps, which proved to be sufficiently long. Longer lifetimes do not lead to distinct changes in the corresponding lifetime value of

TABLE I. Percentages of observed feeding in relation to the total population of the level for the investigated states. In relation to the level excitation energy this value decreases nearly linearly.

State	Energy (keV)	I_{feed}/I_{total}
2_1^+	397.4	59%
4_1^+	938.7	34%
3_1^-	1242.3	15%
6_1^+	1647.8	–
4_2^+	1673.9	–

the 6_1^+ state. With these assumptions, the determined lifetime value for the 6_1^+ state was lowered to $4.8_{-0.7}^{+0.8}$ ps. The lower limit of this result is thus used to correct the lower limit of the uncertainty for $\tau(6_1^+)$. This yields $\tau(6_1^+) = 6.2_{-2.1}^{+1.6}$ ps. Within these uncertainties the given lifetime still holds, even if a large, but still realistic, amount of unobserved feeding was present.

Furthermore a lifetime for the 3_1^- state was obtained. Here the statistics do not allow the determination of both peak components in every single distance with the precision needed for a lifetime analysis. For this reason the method presented in Ref. [10] for obtaining lifetimes from the summed spectra over all distances was used. Here the solution of the summed decay curve, consisting of the Bateman equations of the single distances j,

$$R_{sum} = \frac{\sum_j I_{un,j}}{\sum_j I_{un,j} + \sum_j I_{sh,j}} = \sum_j n_j R(t_{f,j}), \qquad (2)$$

is used, where I_{sh} and I_{un} are the intensities of the shifted and unshifted components of the decay, respectively, t_f denotes the corresponding flight time for every distance x, and n_j is the respective normalization factor. According to Ref. [11] the 3_1^- state receives most of its feeding via the 4_2^+ state with a transition energy of 432 keV. At least an effective lifetime of the feeding state as well as the initial populations of both states are needed for the lifetime determination of the 3_1^-. The $4_2^+ \rightarrow 3_1^-$ transition is observed in the spectrum but is partly overlapped by the contaminating $3_1^- \rightarrow 4_1^+$ transition in ^{142}Ce. This problem could be overcome by using the $3_1^- \rightarrow 2_1^+$ transition in ^{142}Ce, of which only the flight component is visible, and the respective branching from Ref. [12] to correct for the intensity of the contamination. After this correction was applied the effective lifetime of the 4_2^+ state could be determined from the summed spectra, using the method described above. Because no feeding is visible and only an effective lifetime is needed the Bateman equation without feeding assumptions is used. With $R_{sum} = 0.56(7)$, averaged over both detection rings, an effective lifetime $\tau_{eff}(4_2^+) = 27.3_{-6.0}^{+10.9}$ ps is obtained. Graphically this method can be displayed as a $R(\tau)$ curve which is shown in Fig. 6. Uncertainties are again obtained using a Monte Carlo simulation of the analysis process.

The feeding from the 4_2^+ state accounts for 15% of the 3_1^- state's total population, leading to the assumption that direct population accounts for the missing 85%, because no other feeding is visible. According to the feeding percentages of the other states and assuming a first-order dependence of
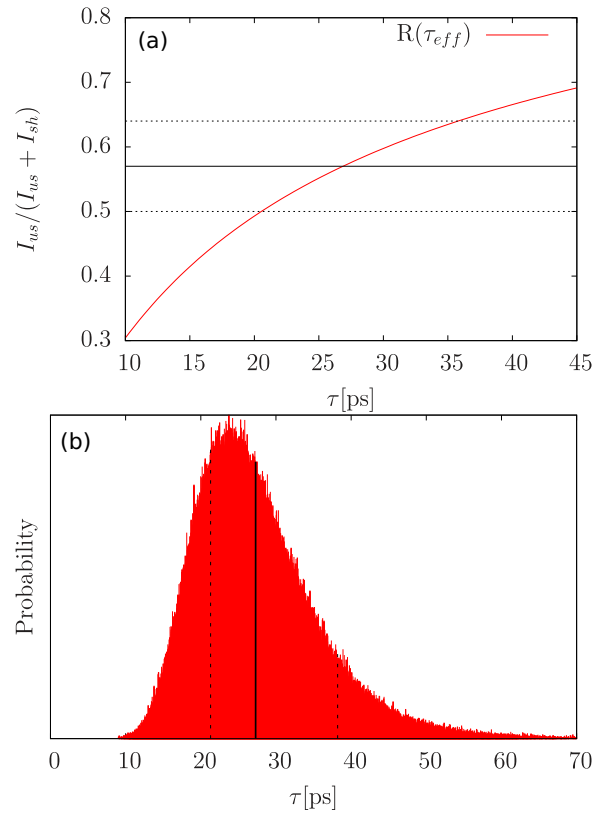

FIG. 6. $R(\tau)$ curve (a) and probability distribution (b) for the 4_2^+ state. See text for details.

the level excitation energy this assumption is realistic. To account for possible unobserved side feeding, additional up to 5% long-lived (100 ps) feeding is assumed for the error calculation via a Monte Carlo simulation. This also accounts for feeding of the 3_1^- state via the 5_1^- state, which could not be observed but can be estimated to be less than 1.5% by using the $5_1^- \rightarrow 4_1^+$ transition and the known branching from Ref. [11]. With $R_{sum} = 0.13(1)$, again, averaged over both detection rings a lifetime of $\tau(3_1^-) = 2.5_{-0.5}^{+0.7}$ ps is obtained. The corresponding $R(\tau)$ curve is shown in Fig. 7. The Monte Carlo simulation to calculate the uncertainties incorporates all mentioned uncertainties of the initial populations as well as

TABLE II. Experimentally obtained lifetime information from this work in comparison to existing values. See text for details.

Decaying State	E_γ (keV)	τ (ps)
2_1^+	397.4	55.1(5)
		52(3)[a]
		42(10)[b]
4_1^+	541.3	$9.4_{-0.4}^{+0.9}$
6_1^+	709.1	$6.2_{-2.1}^{+1.6}$
3_1^-	844.9	$2.5_{-0.5}^{+0.7}$
4_2^+	431.6	27_{-6}^{+11}[c]

[a] Moszynski and Mach [13].
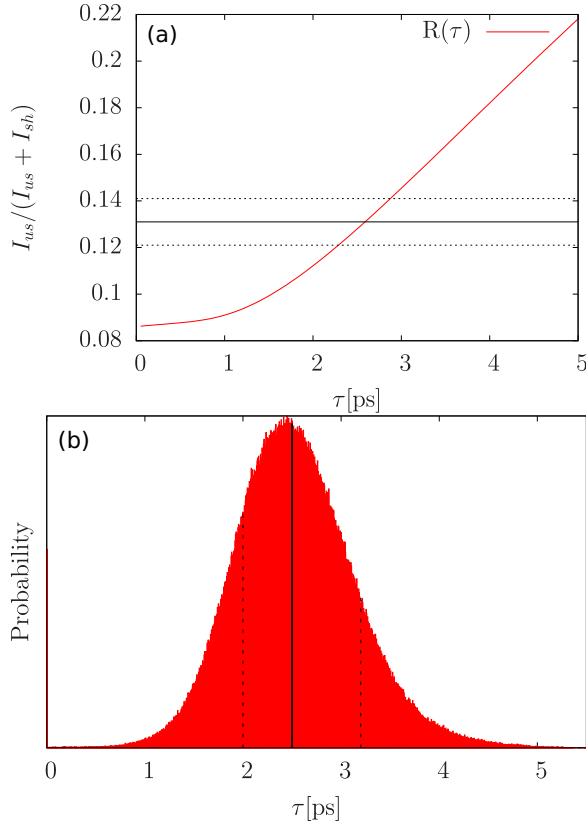[b] Mach *et al.* [14].
[c] Effective lifetime.

FIG. 7. R(τ) curve (a) and probability distribution (b) for the 3_1^- state. See text for details.

the feeding lifetime. All lifetimes resulting from this analysis are summarized in Table II.

IV. DISCUSSION OF THE RESULTS

Prior to this experiment lifetime information of excited states in ^{144}Ce was restricted to the 2_1^+ state, where two lifetime measurements from the year 1989 exist [13,14]. Both measurements used timing techniques (slope method and centroid shift, respectively) from which one agrees with the result obtained here within the error bars. The precision of that lifetime, however, is now improved. All other lifetime information is measured for the first time.

The results of this measurement were used to calculate $B(E2)$ and $B(E1)$ values, assuming pure transitions. For the $6_1^+ \rightarrow 4_1^+$ transition Ref. [11] reports a competing transition to the 5_1^- state with a branching of 0.75(6) (to the 4_1^+ state) and 0.25(6) (to the 5_1^- state), respectively, which was not observed in this experiment. Nevertheless, the literature branching ratio was used to determine the $B(E2, 6_1^+ \rightarrow 4_1^+)$ as well as the $B(E1, 6_1^+ \rightarrow 5_1^-)$ value from the lifetime of the 6_1^+ state. For the 3_1^- state additionally to the $3_1^- \rightarrow 2_1^+$ transition also a transition leading to the 4_1^+ state is reported with a branching of 0.07(2) [11]. Also in this case the branching was used to calculate transition strengths for both transitions. The results are shown in Table III.

In Fig. 8 known $B(E2, 2_1^+ \rightarrow 0_{gs})$ values of the neighboring even-even cerium, barium, and neodymium isotopes

TABLE III. Transition strengths in comparison to shell-model calculations.

Transition	$E\lambda$	$B(E\lambda)(e^\lambda fm^{2\lambda})$ (expt.)	$B(E\lambda)$ $(e^\lambda fm^{2\lambda})$ (theor.[a])
$2_1^+ \rightarrow 0_{gs}^+$	$E2$	1464_{-13}^{+13}	1620
$4_1^+ \rightarrow 2_1^+$	$E2$	1853_{-162}^{+82}	2355
$6_1^+ \rightarrow 4_1^+$	$E2$	537_{-118}^{+289}	2563
$6_1^+ \rightarrow 5_1^-$	$E1$	$(1.3_{-0.4}^{+0.7}) \times 10^{-2}$	–
$3_1^- \rightarrow 4_1^+$	$E1$	$(5.9_{-1.9}^{+2.4}) \times 10^{-4}$	–
$3_1^- \rightarrow 2_1^+$	$E1$	$(3.9_{-0.8}^{+1.0}) \times 10^{-4}$	–

[a]Naïdja *et al.* [11].

are shown together with the newly measured one from this work, beginning at the neutron shell closure at $N = 82$. Up to $N = 88$ the evolution of the $B(E2)$ values can be well described by a linear function, resembling the description of the neutron-deficient isotopes, as displayed in Ref. [15]. This behavior is expected because the collectivity should grow nearly linearly with increasing numbers of valence nucleons for nuclei near closed shells. The abrupt break of the linear behavior, which occurs in the cerium and neodymium chains for $N = 90$ matches with the above mentioned shape phase transition that is expected between $N = 88$ and $N = 90$ [2]. Also this comparison again points out the similarities of the lanthanide nuclei in this mass region.

In the following the results will be discussed in comparison to recent shell-model calculations, which predict $B(E2)$ values in the yrast cascade as well as regarding their impact on the discussion about octupole correlations in ^{144}Ce.

A. Comparison with shell-model calculations

Shell-model calculations for ^{144}Ce, together with ^{142}Ba, were carried out by Naïdja *et al.* in Ref. [11] using the $r4h - r5i$ model space, which consists of the $1f_{7/2}$, $0h_{9/2}$, $1f_{5/2}$, $2p_{3/2}$, $1p_{1/2}$, $0i_{13/2}$ orbitals for neutrons and the $0g_{7/2}$,
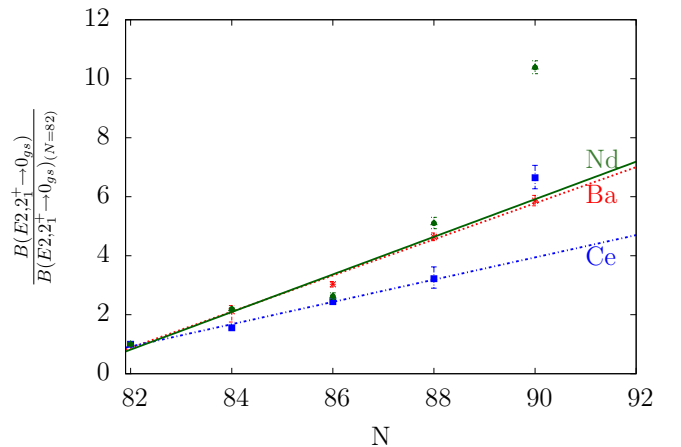

FIG. 8. Systematic of the $B(E2, 2_1^+ \rightarrow 0_{gs})$ values, normalized to the value for $N = 82$, for cerium, barium, and neodymium isotopes above the $N = 82$ shell closure. Data for other Ce isotopes taken from Refs. [16–18]. Data of barium and neodymium isotopes adopted from [8]. The lines are drawn to guide the eye.
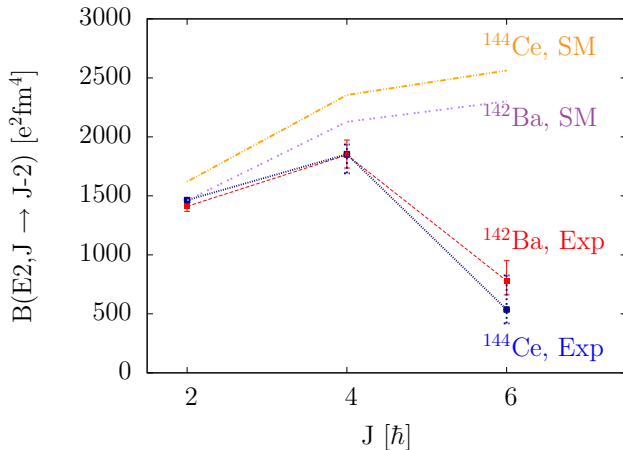
FIG. 9. Comparison of shell-model predictions from Ref. [11] (marked as SM) together with experimentally determined $B(E2)$ transition strengths of ^{144}Ce (from this work) and ^{142}Ba (taken from Refs. [19,21,22]).

$1d_{5/2}$, $1d_{3/2}$, $2s_{1/2}$, $0h_{11/2}$ orbitals for protons and the N3LOP interaction described in Ref. [7]. For ^{144}Ce the occupation numbers of the $0h_{11/2}$ proton orbital and the $0i_{13/2}$ neutron orbital were limited as a necessary truncation. Together with a good reproduction of the level energies of low-lying levels also Q_i values for the yrast cascade up to the 6_1^+ state are given which can be used to deduce the shell-model predictions for the respective $B(E2)$ values. In Table III and Fig. 9 these predictions are compared to the experimental $B(E2)$ values. For the $B(E2)$ values of the $2_1^+ \rightarrow 0_{gs}^+$ and the $4_1^+ \rightarrow 2_1^+$ transitions the trend is well reproduced. The slight overestimation may be from the choice of the effective proton and neutron charges of 1.6e and 0.6e, respectively, in the SM calculation. On the other hand, the shell model is not able to reproduce the sharp drop of the $6_1^+ \rightarrow 4_1^+$ transition strength. For comparison also the $B(E2)$ values for the same transitions in the neighboring isotone ^{142}Ba are shown, together with the respective shell-model predictions from Ref. [11]. As can be seen in Fig. 1, the level structure in the yrast and the supposed octupole band of ^{144}Ce and ^{142}Ba are very alike. Therefore one could expect the same for the behavior of the $B(E2)$ values and indeed the experimental values are nearly identical to the ones from ^{144}Ce including the drop described above. Shell-model predictions are again not able to describe the drop of the $B(E2, 6_1^+ \rightarrow 4_1^+)$. However, it has to be mentioned that the pictured $B(E2)$ value of the $6_1^+ \rightarrow 4_1^+$ transition in ^{142}Ba originates from an experiment, analyzed in a thesis [19], from which the same author in a later paper [20] states that it was not possible to analyze the 6_1^+ state's decay because of potential contaminations. Nevertheless, the comparison here supports the result of that author's first analysis.

B. Octupole deformation

The phenomenon of octupole deformation in atomic nuclei was long under research. Recent experimental results, making use of modern ion beam facilities and detector arrays, have again raised interest by directly measuring octupole $E3$

transition strengths [6,23,24]. Octupole deformation leads to reflection asymmetric nuclear shapes and is mainly indicated by low-lying negative parity bands that alternate with the positive parity yrast bands and fast $E1$ transitions between these bands. The resulting large intrinsic dipole moments D_0 are explained by the displacement from the center-of-mass of proton and neutron densities in asymmetric nuclei [25]. Characteristic $E3$ transitions competing with $E2/E1$ transitions are often too weak to be directly observed but are crucial to determine whether a nucleus exhibits stable octupole deformation or if it behaves like an octupole vibrator. Because this is also the case for ^{144}Ce this discussion is limited to the measured $E1$ transition strengths.

The nucleus ^{144}Ce belongs to the region around $N \approx 88$, $Z \approx 56$, where strong octupole deformation is expected and was, in fact, observed in various numbers of experiments. Prominent examples are the aforementioned measurements described in Refs. [6,23] on ^{144,146}Ba that yielded largely enhanced $E3$ transition strengths. For cerium isotopes calculations done by Agbemava *et al.* within different covariant density functional theory frameworks (namely the covariant energy density functionals DD-PC1 [26], NL3* [27], DD-ME2 [28], PC-PK1 [29], and DD-MEδ [30]) predict strong octupole deformation for $N \geqslant 88$, whereas weaker octupole deformation is already predicted for $N = 86$ [31]. Other recent calculations by Xia *et al.* use a quadrupole-octupole collective Hamiltonian (QOCH) with parameters determined based on the PC-PK1 density functional [32]. The resulting deformation energy surfaces show that ^{144}Ce is expected to be soft on the octupole degree of freedom, but show no finite value of equilibrium octupole deformation. Similar to the calculations by Agbemava *et al.* the latter is predicted for ^{146}Ce and heavier cerium isotopes. Another aspect worth noting is that the deformation energy surfaces shown in Ref. [32] for ^{144}Ce and ^{142}Ba are much alike, as expected from the comparison of the level energies and $E2$ transition strengths shown in Fig. 9.

On the experimental side, the literature reports the yrast low-lying negative parity band in ^{144}Ce to be a good candidate for an octupole deformed band [5]. For states with $J > 5$ it exhibits the typical interspacing of positive and negative parity states together with the positive parity yrast band expected for octupole deformation. To further investigate the case, the experimental observables of choice are the transition strengths between the yrast alternating parity states. These values are significantly enhanced if octupole deformation plays a role. In the case of ^{144}Ce up to now only $E1$ transitions between the bands of interest have been observed. $B(E1)$ transition strengths stronger than $\approx 10^{-5}$ W.u. are an indicator of reflection asymmetry, i.e., octupole deformation [4]. The values measured in this work for the $6_1^+ \rightarrow 5_1^-$, $3_1^- \rightarrow 4_1^+$, and $3_1^- \rightarrow 2_1^+$ transitions certainly fall into that category. Especially the $6_1^+ \rightarrow 5_1^-$ transition strength exceeds the typical range for $E1$ transitions quite drastically. This is best seen when expressed in Weisskopf units, where $B(E1, 6_1^+ \rightarrow 5_1^-) = (7.2^{+2.9}_{-1.9}) \times 10^{-3}$ W.u. It has to be stressed that this value is extremely close to 0.01 W.u., which is the recommended upper limit for $E1$ transitions in this mass region as given in Ref. [33]. This value even exceeds $E1$ strengths in ^{144}Ba, which is assumed to exhibit much stronger octupole deformation [25].

TABLE IV. Experimental intrinsic dipole moments in comparison with theoretical calculations for the given spin ranges.

$I^\pi (\hbar)$	$D_0 (e\text{fm})$ (expt.)	J range$^{\text{theor.}}$	$D_0 (e\text{fm})$ (theor.)[a]
3_1^-	0.06(1)	0	0.17
6_1^+	0.33(9)	5–9	0.20

[a]Butler and Nazarewicz [34].

It is thus an indicator for a very strong collective behavior of this transition.

Furthermore the measured $B(E1)$ values can be used to calculate the intrinsic dipole transition moment D_0 for the respective transitions between the states with the angular momenta I_i and I_f using the formula,

$$D_0^2 = \frac{4\pi}{3} B(E1) \frac{1}{\langle I_i 010 | I_f 0 \rangle^2}, \qquad (3)$$

where $\langle I_i 010 | I_f 0 \rangle$ is the Clebsch-Gordan coefficient. Experimental results for the dipole moments from this work together with theoretical predictions obtained with a shell-correction approach carried out in Ref. [34] are shown in Table IV. To calculate the dipole moment of the 3_1^- state the transition to the 2_1^+ state was used. The dipole moment of the 3_1^- state is compared to the predicted value of the ground state, which is the one given for that spin range in Ref. [34], and is somewhat lower than that value. The one of the 6_1^+ state is remarkably high but not too far away from the predicted value. In the systematic comparisons shown in Ref. [4] and adapted from there in Ref. [32] it can be seen that similarly high dipole moments in octupole candidates have only been measured in ^{152}Sm and the much heavier $^{218-222}$Ra and $^{220-226}$Th isotopes.

Concluding this discussion, the newly measured transition strengths and the calculated transition dipole moments provide a strong indication for the octupole character of the negative parity yrast band in ^{144}Ce. Especially the strong transition between the 6_1^+ and the 5_1^- state matches well with the beginning of the interchanging between positive and negative parity states at these spin values, which is typical for octupole deformation. A structural change at this spin could also possibly explain why the shell-model predictions for this state deviate strongly from the experimental values.

V. CONCLUSION

In summary, studies of transition strengths between yrast states in ^{144}Ce have been carried out by measuring lifetimes of the 2_1^+, 4_1^+, 6_1^+, and 3_1^- states, the last three were determined for the first time, and a new effective lifetime of the 4_2^+ state, using the RDDS method. The newly measured $B(E2, 2_1^+ \rightarrow 0_{gs}^+)$ value fits very well in the systematics of the surrounding neutron-rich cerium isotopes. Furthermore $B(E2)$ values in the ground-state band have been compared to existing shell-model calculations, where a good qualitative agreement up to the $4_1^+ \rightarrow 2_1^+$ transition was found. However, the experimental value for the $6_1^+ \rightarrow 4_1^+$ deviates strongly from the predictions, hinting at a change in the structure of the 6_1^+ state which is not incorporated in the shell model. Lastly, the measured lifetimes were used to get some indications about octupole deformation in ^{144}Ce, by determining $B(E1)$ transition strengths as well as intrinsic transition dipole moments and comparing them to calculations assuming such deformations. The resulting very large values for both properties in comparison to similar nuclei yield a strong backing for the hypothesis that the negative parity yrast band exhibits octupole deformation, especially at higher spins.

To provide further knowledge regarding the question if a nonzero static octupole deformation is present in ^{144}Ce, a measurement of $E3$ transitions has to be carried out. The best candidate is a $3_1^- \rightarrow 0_{gs}^+$ transition, that was observed in many nearby nuclei. However, assuming a $B(E3, 3_1^- \rightarrow 0_{gs}^+)$ value similar to that of other octupole candidates, the expected branching ratio for such a transition would be extremely small. Therefore a measurement employing multistep Coulomb excitation, as described, for example, in Ref. [24], seems to be the most viable method. The lifetimes measured in this work would become extremely useful for such a measurement to restrain the use of free parameters.

[1] J. B. Gupta, Phys. Rev. C **87**, 064318 (2013).

[2] P. Koseoglou, V. Werner, N. Pietralla, S. Ilieva, T. Nikšić, D. Vretenar, P. Alexa, M. Thürauf, C. Bernards, A. Blanc, A. M. Bruce, R. B. Cakirli, N. Cooper, L. M. Fraile, G. de France, M. Jentschel, J. Jolie, U. Köster, W. Korten, T. Kröll, S. Lalkovski, H. Mach, N. Mărginean, P. Mutti, Z. Patel, V. Paziy, Z. Podolyák, P. H. Regan, J.-M. Régis, O. J. Roberts, N. Saed-Samii, G. S. Simpson, T. Soldner, C. A. Ur, W. Urban, D. Wilmsen, and E. Wilson, Phys. Rev. C **101**, 014303 (2020).

[3] P. A. Butler, J. Phys. G: Nucl. Part. Phys. **43**, 073002 (2016).

[4] P. A. Butler and W. Nazarewicz, Rev. Mod. Phys. **68**, 349 (1996).

[5] S. Zhu, Q. Lu, J. Hamilton, A. Ramayya, L. Peker, M. Wang, W. Ma, B. Babu, T. Ginter, J. Kormicki, D. Shi, J. Deng, W. Nazarewicz, J. Rasmussen, M. Stoyer, S. Chu, K. Gregorich, M. Mohar, S. Asztalos, S. Prussin, J. Cole, R. Aryaeinejad, Y. Dardenne, M. Drigert, K. Moody, R. Loughed, J. Wild, N. Johnson, I. Lee, F. McGowan, G. Ter-Akopian, and Y. Oganessian, Phys. Lett. B **357**, 273 (1995).

[6] B. Bucher, S. Zhu, C. Y. Wu, R. V. F. Janssens, D. Cline, A. B. Hayes, M. Albers, A. D. Ayangeakaa, P. A. Butler, C. M. Campbell, M. P. Carpenter, C. J. Chiara, J. A. Clark, H. L. Crawford, M. Cromaz, H. M. David, C. Dickerson, E. T. Gregor, J. Harker, C. R. Hoffman, B. P. Kay, F. G. Kondev,

A. Korichi, T. Lauritsen, A. O. Macchiavelli, R. C. Pardo, A. Richard, M. A. Riley, G. Savard, M. Scheck, D. Seweryniak, M. K. Smith, R. Vondrasek, and A. Wiens, Phys. Rev. Lett. **116**, 112503 (2016).

[7] H. Naïdja, F. Nowacki, and B. Bounthong, Phys. Rev. C **96**, 034312 (2017).

[8] ENSDF database as of october 1st, 2019. Version available at http://www.nndc.bnl.gov/ensarchivals.

[9] A. Dewald, O. Möller, and P. Petkov, Prog. Part. Nucl. Phys. **67**, 786 (2012).

[10] J. Litzinger, A. Blazhev, A. Dewald, F. Didierjean, G. Duchêne, C. Fransen, R. Lozeva, K. Sieja, D. Verney, G. de Angelis, D. Bazzacco, B. Birkenbach, S. Bottoni, A. Bracco, T. Braunroth, B. Cederwall, L. Corradi, F. C. L. Crespi, P. Désesquelles, J. Eberth, E. Ellinger, E. Farnea, E. Fioretto, R. Gernhäuser, A. Goasduff, A. Görgen, A. Gottardo, J. Grebosz, M. Hackstein, H. Hess, F. Ibrahim, J. Jolie, A. Jungclaus, K. Kolos, W. Korten, S. Leoni, S. Lunardi, A. Maj, R. Menegazzo, D. Mengoni, C. Michelagnoli, T. Mijatovic, B. Million, O. Möller, V. Modamio, G. Montagnoli, D. Montanari, A. I. Morales, D. R. Napoli, M. Niikura, G. Pollarolo, A. Pullia, B. Quintana, F. Recchia, P. Reiter, D. Rosso, E. Sahin, M. D. Salsac, F. Scarlassara, P.-A. Söderström, A. M. Stefanini, O. Stezowski, S. Szilner, C. Theisen, J. J. Valiente Dobón, V. Vandone, and A. Vogt, Phys. Rev. C **92**, 064322 (2015).

[11] H. Naïdja, F. Nowacki, B. Bounthong, M. Czerwiński, T. Rzaca-Urban, T. Rogiński, W. Urban, J. Wiśniewski, K. Sieja, A. G. Smith, J. F. Smith, G. S. Simpson, I. Ahmad, and J. P. Greene, Phys. Rev. C **95**, 064303 (2017).

[12] T. Johnson, D. Symochko, M. Fadil, and J. Tuli, Nucl. Data Sheets **112**, 1949 (2011).

[13] M. Moszynski and H. Mach, Nucl. Instrum. Methods A **277**, 407 (1989).

[14] H. Mach, R. Gill, and M. Moszynski, Nucl. Instrum. Methods A **280**, 49 (1989).

[15] A. Dewald, Prog. Part. Nucl. Phys. **28**, 409 (1992).

[16] B. Pritychenko, M. Birch, B. Singh, and M. Horoi, At. Data Nucl. Data Tables **107**, 1 (2016).

[17] R. H. Spear, W. J. Vermeer, S. M. Burnett, G. J. Cyapong, and C. S. Lim, Aust. J. Phys. **42**, 345 (1989).

[18] C. Goodin, J. R. Stone, N. J. Stone, A. V. Ramayya, A. V. Daniel, J. H. Hamilton, K. Li, J. K. Hwang, G. M. Ter-Akopian, and J. O. Rasmussen, Phys. Rev. C **79**, 034316 (2009).

[19] G. Mamane, Ph.D. thesis, Weizmann Institute of Science, Rehovot, 1983.

[20] G. Mamane, E. Cheifetz, E. Dafni, A. Zemel, and J. Wilhelmy, Nucl. Phys. A **454**, 213 (1986).

[21] H. Mach, W. Nazarewicz, D. Kusnezov, M. Moszyn'ski, B. Fogelberg, M. Hellström, L. Spanier, R. L. Gill, R. F. Casten, and A. Wolf, Phys. Rev. C **41**, R2469 (1990).

[22] D. C. Biswas, A. G. Smith, R. M. Wall, D. Patel, G. S. Simpson, D. M. Cullen, J. L. Durell, S. J. Freeman, J. C. Lisle, J. F. Smith, B. J. Varley, T. Yousef, G. Barreau, M. Petit, C. Theisen, E. Bouchez, M. Houry, R. Lucas, B. Cahan, A. Le Coguie, B. J. P. Gall, O. Dorvaux, and N. Schulz, Phys. Rev. C **71**, 011301(R) (2005).

[23] B. Bucher, S. Zhu, C. Y. Wu, R. V. F. Janssens, R. N. Bernard, L. M. Robledo, T. R. Rodríguez, D. Cline, A. B. Hayes, A. D. Ayangeakaa, M. Q. Buckner, C. M. Campbell, M. P. Carpenter, J. A. Clark, H. L. Crawford, H. M. David, C. Dickerson, J. Harker, C. R. Hoffman, B. P. Kay, F. G. Kondev, T. Lauritsen, A. O. Macchiavelli, R. C. Pardo, G. Savard, D. Seweryniak, and R. Vondrasek, Phys. Rev. Lett. **118**, 152504 (2017).

[24] P. A. Butler, L. P. Gaffney, P. Spagnoletti, K. Abrahams, M. Bowry, J. Cederkäll, G. de Angelis, H. De Witte, P. E. Garrett, A. Goldkuhle, C. Henrich, A. Illana, K. Johnston, D. T. Joss, J. M. Keatings, N. A. Kelly, M. Komorowska, J. Konki, T. Kröll, M. Lozano, B. S. Nara Singh, D. O'Donnell, J. Ojala, R. D. Page, L. G. Pedersen, C. Raison, P. Reiter, J. A. Rodriguez, D. Rosiak, S. Rothe, M. Scheck, M. Seidlitz, T. M. Shneidman, B. Siebeck, J. Sinclair, J. F. Smith, M. Stryjczyk, P. Van Duppen, S. Vinals, V. Virtanen, N. Warr, K. Wrzosek-Lipska, and M. Zielińska, Phys. Rev. Lett. **124**, 042503 (2020).

[25] W. R. Phillips, I. Ahmad, H. Emling, R. Holzmann, R. V. F. Janssens, T. L. Khoo, and M. W. Drigert, Phys. Rev. Lett. **57**, 3257 (1986).

[26] T. Nikšić, D. Vretenar, and P. Ring, Phys. Rev. C **78**, 034318 (2008).

[27] G. Lalazissis, S. Karatzikos, R. Fossion, D. P. Arteaga, A. Afanasjev, and P. Ring, Phys. Lett. B **671**, 36 (2009).

[28] G. A. Lalazissis, T. Nikšić, D. Vretenar, and P. Ring, Phys. Rev. C **71**, 024312 (2005).

[29] P. W. Zhao, Z. P. Li, J. M. Yao, and J. Meng, Phys. Rev. C **82**, 054319 (2010).

[30] X. Roca-Maza, X. Viñas, M. Centelles, P. Ring, and P. Schuck, Phys. Rev. C **84**, 054309 (2011).

[31] S. E. Agbemava, A. V. Afanasjev, and P. Ring, Phys. Rev. C **93**, 044304 (2016).

[32] S. Y. Xia, H. Tao, Y. Lu, Z. P. Li, T. Nikšić, and D. Vretenar, Phys. Rev. C **96**, 054303 (2017).

[33] P. Endt, At. Data Nucl. Data Tables **26**, 47 (1981).

[34] P. Butler and W. Nazarewicz, Nucl. Phys. A **533**, 249 (1991).